



# Subtype Diagnosis of Sporadic Creutzfeldt–Jakob Disease with Diffusion Magnetic Resonance Imaging

Alberto Bizzi, MD <sup>1</sup>, Riccardo Pascuzzo, PhD <sup>1</sup>, Janis Blevins, BSc,<sup>2</sup>  
 Marco E. M. Moscatelli, MD <sup>1</sup>, Marina Grisoli, MD,<sup>1</sup> Raffaele Lodi, MD,<sup>3,4</sup>  
 Fabio M. Doniselli, MD,<sup>1</sup> Gianmarco Castelli, MSc,<sup>1</sup> Mark L. Cohen, MD,<sup>2,5,6</sup>  
 Aymeric Stamm, PhD,<sup>7</sup> Lawrence B. Schonberger, MD,<sup>8</sup>  
 Brian S. Appleby, MD,<sup>2,5,6,9</sup> and Pierluigi Gambetti, MD<sup>5</sup>

**Objective:** Sporadic Creutzfeldt–Jakob disease (sCJD) comprises several subtypes as defined by genetic and prion protein characteristics, which are associated with distinct clinical and pathological phenotypes. To date, no clinical test can reliably diagnose the subtype. We established two procedures for the antemortem diagnosis of sCJD subtype using diffusion magnetic resonance imaging (MRI).

**Methods:** MRI of 1,458 patients referred to the National Prion Disease Pathology Surveillance Center were collected through its consultation service. One neuroradiologist blind to the diagnosis scored 12 brain regions and generated a lesion profile for each MRI scan. We selected 487 patients with autopsy-confirmed diagnosis of “pure” sCJD subtype and at least one positive diffusion MRI examination. We designed and tested two data-driven procedures for subtype diagnosis: the first procedure—prion subtype classification algorithm with MRI (PriSCA\_MRI)—uses only MRI examinations; the second—PriSCA\_MRI + Gen—includes knowledge of the prion protein codon 129 genotype, a major determinant of sCJD subtypes. Both procedures were tested on the first MRI and the last MRI follow-up.

**Results:** PriSCA\_MRI classified the 3 most prevalent subtypes with 82% accuracy.

PriSCA\_MRI + Gen raised the accuracy to 89% and identified all subtypes.

Individually, the 2 most prevalent sCJD subtypes, MM1 and VV2, were diagnosed with sensitivities up to 95 and 97%, respectively. The performances of both procedures did not change in 168 patients with longitudinal MRI studies when the last examination was used.

**Interpretation:** This study provides the first practical algorithms for antemortem diagnosis of sCJD subtypes. MRI diagnosis of subtype is likely to be attainable at early disease stages to prognosticate clinical course and design future therapeutic trials.

ANN NEUROL 2020;00:1–13

Sporadic Creutzfeldt–Jakob disease (sCJD) is by far the most common form of human prion disease and has a rapid, progressive clinical course with widespread

deposition of the disease-related prion protein (PrP<sup>D</sup>) in the brain.<sup>1–3</sup> A large phenotypic variability in clinical presentation, disease evolution, and duration has led to the

View this article online at [wileyonlinelibrary.com](http://wileyonlinelibrary.com). DOI: 10.1002/ana.25983

Received Jun 30, 2020, and in revised form Nov 26, 2020. Accepted for publication Nov 29, 2020.

Address correspondence to Dr Bizzi, Neuroradiology Unit, Fondazione IRCCS Istituto Neurologico Carlo Besta, Via Celoria, 11, 20133 Milan, Italy. E-mail: [alberto.bizzi@istituto-besta.it](mailto:alberto.bizzi@istituto-besta.it)

From the <sup>1</sup>Neuroradiology Unit, Fondazione IRCCS Istituto Neurologico Carlo Besta, Milan, Italy; <sup>2</sup>National Prion Disease Pathology Surveillance Center, Case Western Reserve University, School of Medicine, Cleveland, OH; <sup>3</sup>Dipartimento di Scienze Biomediche e Neuromotorie, Università di Bologna, Bologna, Italy; <sup>4</sup>IRCCS Istituto delle Scienze Neurologiche di Bologna, Bologna, Italy; <sup>5</sup>Department of Pathology, Case Western Reserve University, School of Medicine, Cleveland, OH; <sup>6</sup>Department of Neurology, University Hospitals Cleveland Medical Center, Case Western Reserve University, Cleveland, OH; <sup>7</sup>Department of Mathematics Jean Leray, CNRS (National Center for Scientific Research), Nantes, France; <sup>8</sup>National Center for Emerging and Zoonotic Infectious Diseases, Centers for Disease Control and Prevention, Atlanta, GA; and <sup>9</sup>Department of Psychiatry, University Hospitals Cleveland Medical Center, Case Western Reserve University, Cleveland, OH

Additional supporting information can be found in the online version of this article.

description of several clinical variants.<sup>1,4–7</sup> This disease heterogeneity complicates diagnosis, prognosis, treatment, and design and testing of new drugs.<sup>8</sup> It is now well established that sCJD phenotypic heterogeneity is mostly controlled by two determinants: the PrP genotype at the methionine (M) and valine (V) polymorphic codon 129 (determining the MM, MV, and VV genotypes, henceforth denoted *PRNP129*) and the type, 1 or 2, of proteinase K-resistant PrP<sup>D</sup> (resPrP<sup>D</sup>).<sup>9–11</sup> Distinctive molecular subtypes associated with clinicohistopathologic features were identified, each resulting from a specific codon 129 genotype/resPrP<sup>D</sup> type combination with two exceptions. Since the early studies, it has been known that patients with MM1 and MV1 molecular subtypes share the same clinical and histopathologic phenotypes, and, therefore, they have been merged in one subtype, hereafter named MM(V)1.<sup>3,10,12</sup> More recently, the heterozygous MV2 subtype was shown to comprise 2 distinct histopathologic phenotypes or histotypes: one, named MV2C (where C denotes spongiform degeneration in the cerebral cortex) that is virtually the phenocopy of the MM2 subtype; and a second phenotype, named MV2K, that while generally mimicking the VV2 phenotype, differs from it in the presence of prominent kuru (K) plaques.<sup>3,13–15</sup> The 5 sCJD subtypes—MM(V)1, MM(V)2C, VV1, VV2, and MV2K—are associated with distinctive brain lesion distribution profiles.<sup>10</sup> In addition, patients can present 2 subtypes. In these “mixed” cases, the coexistence of 2 disease phenotypes is associated with the presence of both PrP<sup>D</sup> type 1 and 2.<sup>16,17</sup> Commonly, and in this study, the “subtype” term refers to the pairing of genetics and PrP<sup>D</sup> characteristics, whereas “phenotype” refers to clinical and, especially, histopathologic characteristics; however, in the literature they are often used interchangeably. Despite this complexity, the genotype-resPrP<sup>D</sup> type molecular classification of sCJD subtypes is accepted and used worldwide.<sup>3,4,10–13,16</sup>

Impairment of higher cognitive functions, ataxia, and myoclonus are the most common neurological presentation of MM(V)1, MM(V)2C, and VV1, whereas cerebellar ataxia, oculomotor abnormalities, and behavioral disturbances are predominant in VV2 and MV2K.<sup>4</sup> Unfortunately, the large clinical heterogeneity of cognitive, neurological, and behavioral signs prevents precise subtype diagnosis at the bedside. Currently, the individual subtypes of sCJD can be definitively diagnosed only by tissue examination.<sup>2,4</sup> Antemortem diagnosis of the subtype would be helpful for the prognosis, because subtypes have different clinical trajectories as to symptoms and disease duration; furthermore, it would help stratify patients for future drug trials.

Diffusion magnetic resonance imaging (MRI) is one of two excellent diagnostic tests that are currently available for the early diagnosis of sCJD. The other test is real-time quaking-induced conversion (RT-QuIC). This test operates by amplifying minute amounts of PrP<sup>D</sup> and is most often performed with a high degree of sensitivity and specificity on cerebral spinal fluid.<sup>18–20</sup> Unfortunately, until now the diagnosis of subtype with both tests has remained tentative.<sup>21–24</sup>

Advances in diffusion-weighted imaging (DWI) technology have significantly upgraded the diagnostic capabilities of MRI.<sup>25</sup> Along with amendments of its criteria<sup>26,27</sup> and the increasing experience acquired by neuroradiologists, diffusion MRI has become highly reliable in the diagnosis of CJD, despite the rarity of this condition,<sup>21,28,29</sup> reaching sensitivity and specificity values greater than 90%.<sup>1,21,27,30–32</sup> Moreover, MRI plays a pivotal role as an early diagnostic test in patients who present with rapidly evolving signs of cognitive dysfunction, and it can strongly suggest sCJD even before a physician seriously considers this diagnosis.<sup>25</sup> The results of a recent study demonstrated that the sensitivity reached 100% when diffusion MRI and RT-QuIC data were combined.<sup>27</sup>

As a consequence of this high sensitivity, diffusion MRI is probably the best suited technique to detect in vivo the macroscopic topographic distribution of spongiform lesions in the whole brain of patients with distinct sCJD subtypes. In this study, we evaluated the performance of diffusion MRI in diagnosing sCJD subtype in individual patients. Leveraging a large collection of sCJD subjects with diffusion MRI and autopsy-confirmed diagnosis,<sup>27</sup> we used decision tree algorithms that exploited the brain lesion profile of subjects with 5 pure sCJD subtypes. Subjects with mixed phenotypes were not included in this analysis. We trained and tested these data-driven procedures considering two scenarios: the first procedure, which we named prion subtype classification algorithm with MRI (PriSCA\_MRI) is based only on MRI-derived data; the second procedure, PriSCA with MRI and genotype (PriSCA\_MRI + Gen), combines MRI and the *PRNP* codon 129 data. These two procedures with a few straightforward sets of steps provide clinicians with a method to accurately diagnose sCJD subtypes at the bedside of individual patients.

## Materials and Methods

### Patients

Brain MRIs of patients with suspected prion disease were referred to the National Prion Disease Pathology Surveillance Center (NPDPS) in Cleveland, Ohio as part of an MRI consultation service program. We considered a cohort of patients

with multiple MRI examinations that was collected from January 2003 to April 2020 and has been the object of two recently published studies.<sup>27,33</sup> To select subjects for this study, the following two inclusion criteria were applied: (1) autopsy diagnosis of sCJD with a pure subtype (MM1, MM2, MV1, MV2C, MV2K, VV1, and VV2) and (2) MRI study with at least one positive brain region examined on DWI. In the procedure using only MRI data, the two subtypes MM1 and MV1, and likewise MM2 and MV2C, were combined because they share very similar clinicopathological phenotypes and are identified as MM(V)1 and MM(V)2C, respectively. Subjects with the coexistence of 2 or 3 molecular subtypes (ie, MM1 + 2, MV1 + 2 K, MV1 + 2 C, MV1 + 2 K + C, MV2K + C, and VV2 + 1) were excluded. Detailed analysis indicated that type-related features such as disease duration and histopathological characteristics are directly correlated with the relative amount of PrP<sup>D</sup> types 1 and 2.<sup>16</sup> Furthermore, mixed cases with the dominant subtype contributing more than 75% of the total will be classified phenotypically as the dominant subtype.<sup>13,17</sup> We are confident that the exclusion of mixed subtypes will have minor implications for the validity of these models.

This research project was approved by the University Hospitals Cleveland Medical Center Institutional Review Board, and informed consent was waived on deceased subjects for the purpose of this study.

### Diffusion MRI Evaluation

An expert neuroradiologist (15 years of experience) prospectively had scored all diffusion MRIs in electronic format, blind to the clinical data and preliminary diagnosis, and generated one lesion profile for each MRI study by evaluating the presence of DWI signal hyperintensities in 12 brain regions on a 4-point ordinal scale, as previously described.<sup>27</sup> Five neocortical regions (frontal, temporal, parietal including the precuneus, and occipital lobes), 3 limbic structures (cingulate, insula, and hippocampus), striatum (caudate and putamen), thalamus, and cerebellum were evaluated. Fluid-attenuated inversion recovery images were systematically inspected before DWI in all patients; DWI signal hyperintensities were confirmed as areas of low diffusivity on apparent diffusion coefficient maps. Presence or absence of symmetry of the DWI abnormalities was noted. When both sides of the brain were affected, the neuroradiologist labeled the DWI abnormalities as asymmetric if one cerebrum was affected more extensively than the contralateral.

The MRI diagnosis of sCJD was made applying the new recently proposed criterion.<sup>27</sup>

In a previous study, we reported that the interrater agreement among 4 neuroradiologists who generated the DWI lesion profile applying the same criteria used in this study was excellent in the scores, with intraclass correlation coefficient between 0.86 and 0.93 in 6 of 12 brain regions.<sup>27</sup>

### Neuropathology

All autopsy studies were performed at the NPDPC and typically included histopathological and PrP<sup>D</sup> immunohistochemical examinations of 17 and 8 brain regions, respectively, as well as

PrP gene and resPrP<sup>D</sup> Western blot analyses in at least 3 brain regions designed to achieve the final diagnosis of sCJD subtype. Diagnosis of sCJD subtype was initially established by a senior neuropathologist and reviewed along with the Western blot by a second neuropathologist, who finalized it.<sup>9–11</sup> “Pure” subtype of sCJD was defined by the lack of any histopathological, immunohistochemical and Western blot evidence of coexistence of two types.<sup>3</sup>

### Statistical Analysis

We adopted a machine learning method known as Classification and Regression Tree (CART)<sup>34</sup> to classify subtypes of sCJD following 2 scenarios: examination of first MRI alone or combined with *PRNP129*. For the first scenario, we used one decision tree that used only MRI data, named PriSCA\_MRI. For the second scenario, we used PriSCA\_MRI + Gen, with one decision tree for each of 3 *PRNP129* genotypes.

In both scenarios, the decision tree relied on the answers to a series of questions related to the distribution of DWI abnormalities, to split the patient population in progressively more homogeneous groups, each ideally belonging to the same sCJD subtype. Each diagnostic algorithm was trained and optimized on about 62% of the data ( $n = 301$ , training set) relative to the first MRI examination with at least one positive brain region, using the “caret” R package (v6.0.76) with the “rpart” method.<sup>35</sup> We used the Gini impurity index to choose the candidate splits used to grow the tree at each step, and we selected the best complexity parameter (cp) that minimized the classification error computed by a leave-one-out cross-validation procedure. No further splits were performed when subsequent divisions did not decrease the classification error of a factor of cp.

The classification performance of each diagnostic algorithm was tested on the remaining 38% of the data ( $n = 186$ , test set) by computing the sensitivities of each subtype and the overall accuracy as a weighted average of the sensitivities, using the frequencies of the subtypes in the sCJD population as weights.<sup>4</sup> We used the following cutoffs to assess the classification performances of the algorithms: high (>85%), good (70–85%), poor/nondiagnostic (<70%). The sizes of training and test sets were chosen according to the golden proportion (ie, the ratio between total sample size and training set size is the same as the ratio between training set size and test set size). Data splitting into training and test sets was performed randomly, checking that the two sets had similar distribution of sCJD subtype (Fisher test,  $p = 0.261$ ), homogeneous median age (65 years, interquartile range [IQR] = 59–72, in both sets; Wilcoxon rank sum test  $p = 0.964$ ), and similar disease duration (4.0, IQR = 2.6–7.3 and 4.4, IQR = 2.4–9.7 months, respectively; Wilcoxon rank sum test  $p = 0.304$ ). Wilcoxon rank sum test was used to test differences in disease intervals (ie, time from onset to MRI, time from MRI to death, and total disease duration) between groups. Bonferroni procedure was used to correct for multiple comparisons. McNemar test was used to compare classification accuracies between PriSCA\_MRI and PriSCA\_MRI + Gen in the test set, accounting for use of the same subjects. Fisher test

was used to compare classification accuracies of each procedure between training and test sets.

In the cohort of patients with multiple MRI studies, we investigated how many patients presented with a different lesion profile on the last follow-up MRI, and how the new lesions affected the subtype classification. Patients were reclassified with PriSCA\_MRI and PriSCA\_MRI + Gen according to the DWI lesion scores of their last MRI study. Then we applied McNemar test to compare the classification accuracies of the two procedures at first and last MRI, accounting for use of the same subjects.

Finally, we determined the percentage of new DWI signal abnormalities occurring in the 12 brain regions in the last MRI for each sCJD molecular subtype. We used Fisher test to verify whether they were different among subtypes.

Statistical significance level was set at 2-sided  $p < 0.05$ . Statistical analyses were done in R, version 3.6.0 (R Foundation for Statistical Computing, Vienna, Austria).

## Results

The patients flow chart illustrating the recruiting process of the cohort of 487 subjects with autopsy-confirmed diagnosis of the 5 pure sCJD subtypes from the originally recruited 1,458 patients with suspected prion disease, and the demographics of the selected subjects are respectively shown in Figure 1 and Table 1. The brain lesion profile generated from each diffusion MRI examination available for each subject was used for the analysis. The MRI diagnoses of subtype were made by using 2 data-driven procedures: one based on the score of the diffusion MRI alone (PriSCA\_MRI), the other supplemented by *PRNP129* genotyping data (PriSCA\_MRI + Gen).

At first MRI scan, the overall accuracy of PriSCA\_MRI with the test set was 82% (Table 2). The accuracy of PriSCA\_MRI + Gen with the test set was 89%, significantly higher ( $p < 0.001$ , odds ratio 95% confidence interval [CI] = 1.90–13.78) than that of PriSCA\_MRI (Table 3). Concerning the most prevalent subtypes, PriSCA\_MRI and PriSCA\_MRI + Gen, respectively, achieved diagnostic sensitivities of 89 and 95% in MM1, 84 and 97% in VV2, and 64 and 57% in MV2K. Furthermore, the PriSCA\_MRI + Gen procedure could also diagnose the rarer MV2C and VV1 with 76 and 92% sensitivity, respectively (see Table 3).

The overall accuracy of both procedures did not significantly vary when the test results were compared with those of the training set (81 and 87% with  $p = 0.336$ , odds ratio 95% CI = 0.52–1.26 and  $p > 0.999$ , odds ratio 95% CI = 0.58–1.69, respectively; Tables S1 and S2). Furthermore, the accuracy of both procedures did not significantly change when the last diffusion MRI scan of the 168 patients, who underwent follow-up studies, was used rather than the first MRI; the accuracies of PriSCA\_MRI and PriSCA\_MRI + Gen were 80% ( $p = 0.118$ , odds ratio

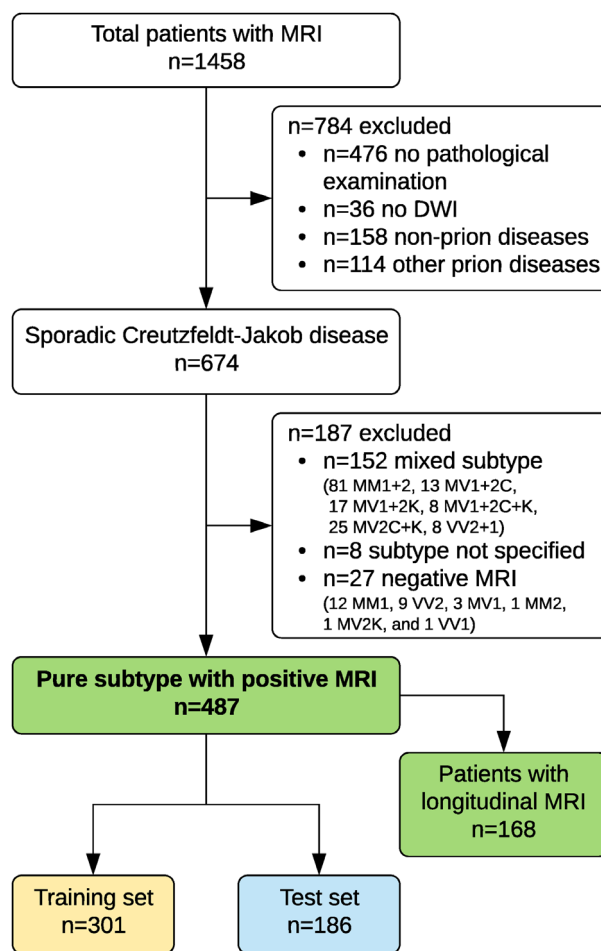


**FIGURE 1:** Flow chart of the patients with suspected diagnosis of sporadic Creutzfeldt-Jakob disease (sCJD) recruited in the study. The diagram illustrates the sequential steps followed to select and characterize the cohort used in the analysis. The number of patients is indicated in each box. Included patients had (1) pure sCJD subtype confirmed at autopsy and (2) at least one positive magnetic resonance imaging (MRI) with diffusion-weighted imaging (DWI).

95% CI = 0.13–1.19) and 87% ( $p = 0.814$ , odds ratio 95% CI = 0.27–2.25), respectively.

### Subtype Diagnosis by Diffusion MRI Alone

The PriSCA\_MRI procedure consists of a decision tree with 2 branches and 7 terminal nodes (Fig 2). The design of the tree was driven by the lesion profile scores of the first MRI scan, which were obtained from a training set of 301 subjects (62% of the cohort).

As expected, the use of MRI data alone did not separate subtypes with similar topographic distribution of the brain pathology; thus, VV1 could not be distinguished from MM(V) 1 and MM(V)2C, and MV2K from VV2. However, whereas VV2 and MV2K were assigned to the same terminal nodes (1 and 7), patients with the very rare VV1 subtype were scattered in several terminal nodes, and they could not be identified in the

**TABLE 1. Demographics of 487 Patients with Autopsy-Confirmed Diagnosis of Sporadic Creutzfeldt–Jakob Disease Subtype**

Molecular Subtype	n (%)	M/F	Age at Onset, Median (IQR) yr	Disease Duration, Median (IQR) mo	Time from Onset to First MRI, Median (IQR) days	MRI Examined, n
MM1	215 (44.1)	114/101	66 (59–73)	2.6 (2.0–3.4)	47 (30–68)	328
MV1	40 (8.2)	22/18	67 (57–70)	4.1 (2.6–10.4)	69 (42–112)	58
MM2	43 (8.8)	20/23	66 (58–73)	12.5 (5.6–23.4)	86 (38–238)	59
MV2C	37 (7.6)	16/21	65 (61–69)	16.9 (9.8–24.2)	109 (54–285)	57
MV2K	36 (7.4)	20/16	64 (59–69)	12.2 (6.8–15.8)	158 (93–317)	49
VV1	25 (5.1)	13/12	56 (41–69)	9.7 (5.7–13.2)	120 (57–167)	31
VV2	91 (18.7)	43/48	65 (59–71)	5.0 (4.2–6.7)	99 (61–133)	129

F = female; IQR = interquartile range; M = male; MRI = magnetic resonance imaging.

**TABLE 2. Case Distribution and Prevalence along with Overall and Individual Diagnostic Accuracies of sCJD Subtypes Achieved with PriSCA\_MRI Performed on sCJD Test Set Subjects**

PriSCA_MRI	Autopsy				
	MM(V)1	MM(V)2C	VV1	MV2K	VV2
MM(V)1	81 <sup>a</sup>	18	10	5	5
MM(V)2C	6	18 <sup>a</sup>	2	0	0
VV2 or MV2K	4	2	0	9 <sup>a</sup>	26 <sup>a</sup>
Sensitivity per subtype	89.0% (81/91)	47.4% (18/38)	0% (0/12)	64.3% (9/14)	83.9% (26/31)
Specificity per subtype	60.0% (57/95)	94.6% (140/148)	100% (174/174)	96.5% (166/172)	90.3% (140/155)
Subtype prevalence <sup>b</sup>	66%	9%	1%	6%	18%
Overall accuracy	82.0%				

Data refer to numbers of patients, unless otherwise specified. The first 3 rows show the subtype case distribution as classified by the PriSCA\_MRI algorithm (first column) and compared with autopsy-established subtypes (table header). The rare VV1 subtype could not be identified by the algorithm. Sensitivity and specificity are reported for each subtype. The specificity for a subtype is the percentage of patients correctly identified among those with other subtypes. The overall accuracy of PriSCA\_MRI (last row) is computed as a weighted average of the sensitivities per subtype, using the subtype prevalence in the sCJD population as weights.

<sup>a</sup>These cells identify PriSCA\_MRI correct diagnoses for each sCJD subtype. On the same rows, other cells denote misclassifications.

<sup>b</sup>Pure subtype prevalence does not include patients with mixed phenotypes<sup>4</sup>.

PriSCA\_MRI = prion subtype classification algorithm with magnetic resonance imaging; sCJD = sporadic Creutzfeldt–Jakob disease.

decision tree elaborated by PriSCA\_MRI, probably due to the insufficient number of VV1 subjects in the training set.

Internal nodes 1 and 2 emerged as pivotal players in the diagnostic process. The first separates cases according to the presence of signal abnormalities in the cerebral cortex leading to the initial diagnosis of the VV2 and MV2K subtypes with combined positive predictive value (PPV) of 91%. Internal node 2, which is based on the presence of

DWI abnormality in the striatum, engendered 2 arms of the diagnostic tree, both of which contribute to the diagnosis of the MM(V)1 subtype with a cumulative PPV of 65% for the left arm (83/128 patients) and 78% for the right arm (141/180 patients). Furthermore, the left arm leads to the diagnosis of the rare MM(V)2C subtype with a PPV of 60% and the right contributes cases to the VV2/MV2K diagnostic group with a 74% PPV.

**TABLE 3. Case Distribution and Prevalence along with Overall and Individual Diagnostic Accuracies of sCJD Subtypes Achieved with PriSCA\_MRI + Gen Performed on sCJD Test Set Subjects**

MM Genotype	MV Genotype			VV Genotype					
	Autopsy		PriSCA_MRI + Gen	Autopsy		PriSCA_MRI + Gen	Autopsy		
PriSCA_MRI + Gen	MM1	MM2		MV1	MV2C		MV2K	VV1	VV2
MM1	73 <sup>a</sup>	7	MV1	8 <sup>a</sup>	5	5	VV1	11 <sup>a</sup>	1
MM2	4	10 <sup>a</sup>	MV2C	5	16 <sup>a</sup>	1	VV2	1	30 <sup>a</sup>
			MV2K	1	0	8 <sup>a</sup>			
Sensitivity per subtype	94.8% (73/77)	58.8% (10/17)		57.1% (8/14)	76.2% (16/21)	57.1% (8/14)		91.7% (11/12)	96.8% (30/31)
Specificity per subtype	58.8% (10/17)	94.8% (73/77)		71.4% (25/35)	78.6% (22/28)	97.1% (34/35)		96.8% (30/31)	91.7% (11/12)
Prevalence <sup>b</sup>	61%	4%		5%	5%	6%		1%	18%
Overall accuracy	88.6%								

Data refer to numbers of patients, unless otherwise specified. In each genotype, the first 2 (3 for MV) rows show the subtype case distribution as classified by the (PriSCA\_MRI + Gen) algorithm (first column of each genotype table) and compared with autopsy-established subtypes (table header). Sensitivity and specificity are reported for each subtype. The specificity for a subtype is the percentage of patients correctly identified among those with other subtypes. The overall accuracy of PriSCA\_MRI + Gen (last row) is computed as a weighted average of the sensitivities per subtype, using the subtype prevalence in the sCJD population as weights.

<sup>a</sup>These cells identify (PriSCA\_MRI + Gen) correct diagnoses for each sCJD subtype. On the same rows, other cells denote misclassifications.

<sup>b</sup>Pure subtype prevalence does not include patients with mixed phenotypes<sup>4</sup>.

PriSCA\_MRI + Gen = prion subtype classification algorithm with magnetic resonance imaging and *PRNP129* genotype; sCJD = sporadic Creutzfeldt–Jakob disease.

The seemingly contradictory finding that different internal nodes lead to the same diagnosis, as is the case of MM(V)1, which is selected in 4 terminal nodes and of VV2/MV2K, which is selected in two, prompted us to investigate whether there were differences in time from clinical onset to MRI between the groups (Table 4). MM(V)1 patients with striatal lesions (terminal nodes 5 and 6) had a longer time interval between clinical onset and first MRI (median = 55 days, IQR = 36–77) and shorter time from first MRI to death (24 days, IQR = 16–36) than those without (terminal nodes 2 and 3: 36 days, IQR = 22–55 and 40 days, IQR = 24–53, respectively;  $p = 0.001$ , 95% CI of the difference = 9–25 days and  $p < 0.001$ , 95% CI of the difference = 8–18 days, respectively), although total disease duration was similar in these 2 groups. These findings support the conclusion that in MM(V)1 patients, the striatum is affected later than the cerebral cortex (dashed arrows in Fig 2) and that the timing of the brain MRI scan determines whether patients with MM(V)1 are diagnosed in the left or right arm of the decision tree.

The time from symptom onset to first MRI was also shorter in the VV2 and MV2K patient groups with no cortical pathology (terminal node 1) compared with the group showing 1 or 2 symmetric cortical lesions (terminal

node 7), although the low number of subjects prevented reaching statistical significance (see Table 4).

### Diagnosis by Diffusion MRI and PRNP129

Diffusion MRI complemented by information on the patient's *PRNP129* required a decision tree for each of the 3 genotypes. The striatum was the key lesion for the MM genotype (Fig 3A). MM1 associated with striatal abnormalities reached a PPV of 98% (125/128). When the striatum was spared, MM1 was distinguished from the MM2 subtype through the same 2 internal nodes as those of the left arm of PriSCA\_MRI. This selection led to the identification of striatum-negative MM1 cases with PPV of 83 and 81%, respectively, whereas the rare MM2 subtype, which by and large share the topography of the spongiform degeneration with MM1, reached a PPV of 60% (24/40), almost 7 times greater than the general frequency (8.8%) of this subtype in our cohort.

The parietal cortex, striatum, and thalamus emerged as 3 key lesions for distinguishing the subtypes sharing the MV genotype (see Fig 3B). The decision tree led most successfully to the diagnosis of MV2K subtype (PPV of 86%; 25/29) when patients showed the association of thalamic lesions with sparing of the parietal cortex. The rare MV2C subtype was diagnosed with a PPV of 67%

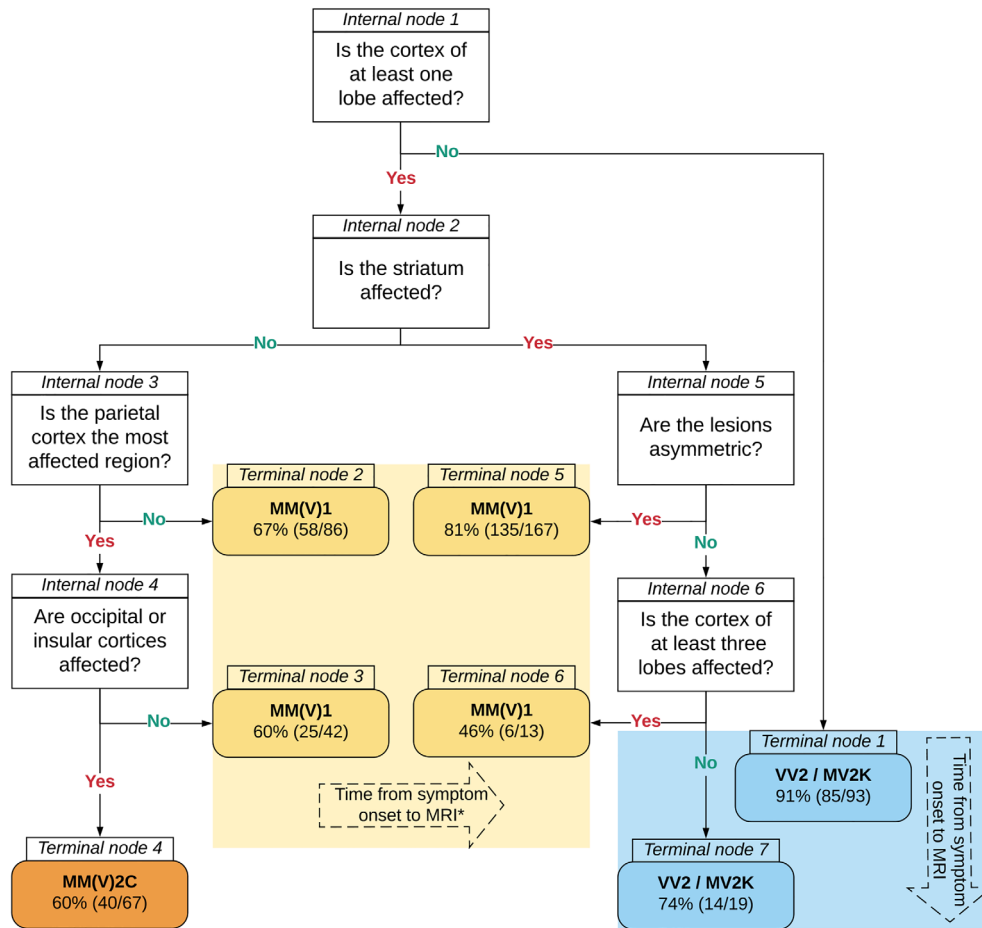


**FIGURE 2: Algorithm for diagnosis of sporadic Creutzfeldt-Jakob disease (sCJD) subtype with magnetic resonance imaging (MRI) alone (PriSCA\_MRI).** The queries in the internal nodes (white boxes) outline the decision tree and lead to either the subtype diagnosis in the terminal node (colored boxes) or to additional queries directed at further defining MRI lesions and diagnoses. In each terminal node, the positive predictive value is indicated along with the number of patients for the most frequent sCJD subtype over the total patients assigned to that node. The large dashed arrows in the yellow and cyan boxes indicate the time increase from symptom onset to first MRI examination related to MM(V)1 and VV2 or MV2K patients, respectively. Asterisk indicates a significant time increase ( $p = 0.001$ ) for MM(V)1 subtype.

(29/43) in the presence of signal abnormality in the parietal cortex but not in the striatum.

Both subtypes sharing the VV genotype scored well based on thalamic and cerebral cortical lesion profile (see Fig 3C). The PPV for VV2 subtype was 100% (50/50) when the thalamus was affected and 95% (35/37) when the thalamus was spared and the cortical ribbon involvement was limited to one lobe. By contrast, normal thalamus and widespread DWI signal hyperintensity in the cortex identified the very rare VV1 subtype with a PPV of 79% (23/29).

### **Evolution of DWI Abnormalities in Patients with Follow-up MRI Studies**

Multiple MRI examinations were available in 34% (168/487) of sCJD patients, the large majority of which were acquired within 3 months from the first MRI scan (88%, 148/168; median after 22 days, IQR = 9–48). At

least one new abnormal region on DWI was identified in 48% (80/168) of subjects, uniformly distributed within the first 90 days for all sCJD subtypes. VV2 was the subtype with the highest detection rates of new abnormal regions (67%, 20/30), but the rate was not significantly different among subtypes (Table 5).

The appearance of new abnormal regions on DWI between the first and last MRI significantly differed among sCJD subtypes and impacted 3 brain regions (see Table 5): the thalamus, which became abnormal in patients with VV2 and MV2K subtypes only; the precuneus and the temporal cortex, which were more frequently affected in MM(V)1 and MM(V)2C than in VV2 and MV2K. Of note, on first MRI the parietal lobe was already abnormal in 96% (24/25) of patients with MM(V)2C, suggesting the disease process impacts this brain region very early in this subtype. The caudate was the region most frequently showing new DWI

**TABLE 4. The Occurrence of DWI Abnormalities in the Striatum of MM(V)1 and in the Neocortex of VV2 and MV2K Patients Is Associated with the Timing of the MRI**

		MM(V)1		VV2		MV2K	
DWI abnormalities		Striatum		Cortex		Cortex	
		-	+	-	+	-	+
Patients, n		141	83	65	9	20	5
Time intervals, days	From clinical onset to first MRI	36 (22–58) <sup>a</sup>	55 (36–77) <sup>a</sup>	97 (61–131)	116 (85–212)	143 (47–192)	328 (317–389)
	Adjusted p	0.001 <sup>a</sup>		>0.999		0.841	
	From first MRI to death	40 (24–53) <sup>a</sup>	24 (16–36) <sup>a</sup>	57 (32–78)	58 (25–81)	131 (84–205)	86 (49–132)
	Adjusted p	<0.001 <sup>a</sup>		>0.999		>0.999	
Total disease duration		81 (57–104)	81 (64–108)	145 (120–194)	153 (141–257)	260 (165–403)	377 (366–475)
	Adjusted p	>0.999		>0.999		0.998	

Data are median values, with interquartile range in parentheses, unless otherwise specified. Groups of patients were identified by prion subtype classification algorithm with MRI (see Fig 2). Time intervals are compared between groups of patients without (–) or with (+) DWI abnormalities in key brain regions.

<sup>a</sup>Significant differences (adjusted  $p < 0.05$  with Bonferroni correction).

DWI = diffusion-weighted imaging; MRI = magnetic resonance imaging.

abnormalities, which, however, did not significantly differ among subtypes.

Using the last MRI in place of the first MRI scan, the subtype diagnosis did not change in 88% (148/168) of patients with PriSCA\_MRI and in 89% (150/168) with PriSCA\_MRI + Gen. The subtype diagnosis from first to last MRI changed in 20 and 18 patients with PriSCA\_MRI and PriSCA\_MRI + Gen, respectively; 14 and 10 patients were correctly diagnosed with the first MRI, whereas 6 and 8 patients were correctly assigned with the last MRI, respectively.

## Discussion

The early diagnosis of sCJD subtypes is clinically relevant not only because the subtypes significantly differ as to survival time and lesion propagation in the brain,<sup>33</sup> but also because evidence indicates that subtypes may respond differently to drug treatment.<sup>36,37</sup> This notion implies that, once treatments become available, they may have to be tailored to the sCJD subtype. Furthermore, subtype diagnosis is also relevant for informing the family about expected survival time. The current lack of a robust, early, and noninvasive diagnostic procedure of sCJD subtype applicable to individual patients prompted us to test data-driven algorithms in the form of decision trees on a large patient cohort. This approach, along with the application

of the MRI lesion profile based on the distribution of DWI abnormalities in 12 brain regions, led to the identification of individual sCJD subtypes with high diagnostic accuracies that were maintained in the follow-up MRI examinations. The most prevalent MM1 and VV2 subtypes, which combined account for nearly 80% of all sCJD subtypes, were diagnosed with high degrees of accuracy by PriSCA\_MRI (89 and 84%) and PriSCA\_MRI + Gen (95 and 97%). Notably, the rare subtypes VV1 and MV2C were also identified by PriSCA\_MRI + Gen with high and good accuracies (92 and 76%). Overall, these findings show that our decision trees can capture the heterogeneity of sCJD by identifying the key brain lesions that best distinguish the 5 pure subtypes, regardless of the time interval between clinical presentation and acquisition of the MRI study.

The decision trees are not only robust but also practical and easily usable at the bedside. This is the advantage of the CART method, which is not a black box, in contrast to other popular algorithms. For instance, the interpretation of the results achieved with random forest, support vector machine, or deep learning techniques is difficult because easy-to-follow steps to classify the subtype of an individual patient are lacking. On the contrary, our procedures provide reliable and direct support to the clinicians without the need for any preprocessing step or the use of dedicated software as required by the other methods.

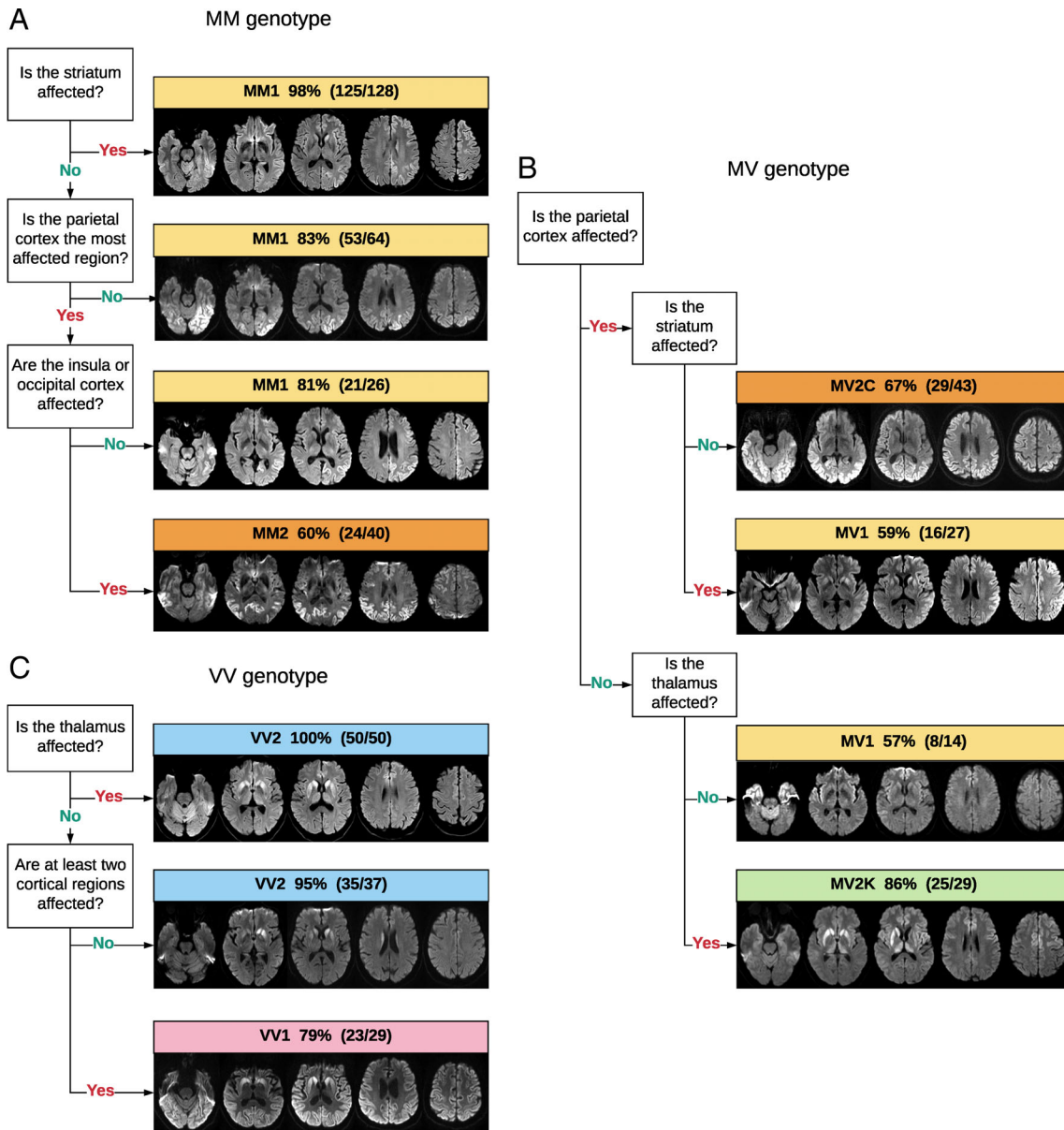


**FIGURE 3:** Algorithms for diagnosis of sporadic Creutzfeldt-Jakob disease (sCJD) subtype with magnetic resonance imaging (MRI) and genotype (PriSCA\_MRI + Gen). The queries in the internal nodes (white boxes) outline the decision tree and lead to either the subtype diagnosis in the terminal node (colored boxes) or to additional queries. In each terminal node, the positive predictive value is indicated with the number of patients for the most frequent sCJD subtype over the total patients assigned to that node. Five axial diffusion-weighted imaging (DWI;  $b = 1,000$ ) sections at the level of the temporal lobes, striatum, thalamus, insula, and occipital, temporal, frontal, and parietal lobes of a typical case are illustrated for each terminal node. (A) From top to bottom, in the first terminal node (MM1), note the DWI signal hyperintensities in the caudates and asymmetric extensive cortical hyperintensities. In the second terminal node, there is no evidence of abnormality in the striatum; the cortical abnormalities in the left occipital cortex are more extensive than in the parietal cortex. In the third terminal node, the left parietal cortex is the most affected region, but the insula and the occipital cortex are spared (as well as the striatum). In the last terminal node (MM2), the striatum is spared, the left parietal cortex is the most affected region, and the right insula and the bilateral occipital cortex are also affected. In all cases, note susceptibility artifacts in the temporal lobes. (B) In the first terminal node (MV2C), note the extensive bilateral parietal cortical hyperintensities and lack of striatal involvement. In the second terminal node (MV1), there are hyperintensities in the left frontal, parietal, and temporal cortices and in the bilateral striata. In the third terminal node (MV1), the parietal cortex and thalami are spared. However, there are bilateral signal hyperintensities in the cingulate, insula, cortical ribbon of the frontal and temporal lobes, and cerebellum. In the last terminal node (MV2K), the parietal cortex is spared, and the thalami are affected. In addition, there are signal hyperintensities in the striatal nuclei bilaterally, cingulate, and cortical ribbon of the frontal lobes. In all cases, note susceptibility artifacts in the temporal lobes. (C) In the first terminal node (VV2), note the bilateral signal thalamic hyperintensities. In addition, there are bilateral signal hyperintensities in the striata, cingulate, and cerebellum. In the second terminal node (VV2), the thalami and the whole cortex are spared. Bilateral abnormalities are recognized in the striata. In the last terminal node (VV1), the thalami are spared, and bilateral cortical hyperintensities are present in 4 lobes (as well as in the striata). In all cases, note susceptibility artifacts in the temporal lobes.

**TABLE 5. Occurrence of New Brain Regional Abnormalities Detected on DWI after the First MRI in sCJD Molecular Subtypes**

Brain Region	Molecular Subtype							Adjusted <i>p</i> (comparison among all subtypes)	All sCJD Subtypes Combined
	MM1	MV1	MM2	MV2C	MV2K	VV1	VV2		
n	82	16	13	12	11	4	30		168
Frontal	44% (7/16)	67% (2/3)	50% (3/6)	75% (3/4)	20% (1/5)	(0/0)	12% (3/26)	0.158	32% (19/60)
Temporal	<b>22% (10/46)<sup>a</sup></b>	<b>80% (4/5)<sup>a</sup></b>	<b>50% (2/4)<sup>a</sup></b>	<b>100% (1/1)<sup>a</sup></b>	0% (0/7)	(0/0)	4% (1/28)	0.003 <sup>b</sup>	20% (18/91)
Precuneus	<b>45% (5/11)<sup>a</sup></b>	<b>60% (3/5)<sup>a</sup></b>	<b>67% (2/3)<sup>a</sup></b>	<b>100% (3/3)<sup>a</sup></b>	0% (0/8)	<b>100% (1/1)<sup>a</sup></b>	4% (1/25)	<0.001 <sup>b</sup>	27% (15/56)
Parietal	33% (4/12)	67% (2/3)	(0/0)	100% (1/1)	25% (2/8)	100% (1/1)	7% (2/27)	0.062	23% (12/52)
Occipital	11% (7/65)	0% (0/10)	33% (3/9)	29% (2/7)	0% (0/10)	0% (0/3)	0% (0/29)	0.293	9% (12/133)
Cingulate	44% (14/32)	0% (0/5)	0% (0/8)	38% (3/8)	43% (3/7)	(0/0)	29% (5/17)	>0.999	32% (25/77)
Insula	16% (8/49)	22% (2/9)	14% (1/7)	38% (3/8)	11% (1/9)	(0/0)	20% (5/25)	>0.999	19% (20/107)
Hippocampus	7% (5/75)	0% (0/13)	8% (1/12)	0% (0/10)	0% (0/10)	50% (1/2)	15% (4/26)	>0.999	7% (11/148)
Caudate	42% (18/43)	13% (1/8)	17% (2/12)	18% (2/11)	0% (0/3)	67% (2/3)	57% (4/7)	>0.999	33% (29/87)
Putamen	27% (16/60)	20% (2/10)	8% (1/12)	9% (1/11)	0% (0/3)	50% (1/2)	60% (9/15)	0.367	27% (30/113)
Thalamus	0% (0/80)	0% (0/14)	0% (0/11)	0% (0/12)	<b>33% (1/3)<sup>a</sup></b>	0% (0/4)	<b>42% (8/19)<sup>a</sup></b>	<0.001 <sup>b</sup>	6% (9/143)
Cerebellum	4% (3/73)	0% (0/13)	8% (1/13)	0% (0/12)	0% (0/9)	0% (0/3)	24% (4/17)	>0.999	6% (8/140)
At least 1 region	44% (36/82)	31% (5/16)	46% (6/13)	50% (6/12)	45% (5/11)	50% (2/4)	67% (20/30)	0.345	48% (80/168)

For each brain region, the ratio reported in parentheses refers to the number of patients with a new DWI abnormality in that region at last MRI over the number of patients having that region normal at first MRI.

<sup>a</sup>Bold value cells indicate regions with significant differences among subtypes.

<sup>b</sup>Significant comparisons are indicated in the column reporting the adjusted *p* values (Bonferroni correction applied).

DWI = diffusion-weighted imaging; MRI = magnetic resonance imaging; sCJD = sporadic Creutzfeldt–Jakob disease.

Only one comprehensive study, by Meissner and colleagues, has previously attempted to describe MRI lesions distribution according to subtype across the entire phenotypic spectrum of sCJD.<sup>23</sup> This study and ours differ in several methodological aspects. First, Meissner and colleagues relayed on a binary approach rather than the linear score of our study. Second, they predicted resPr<sup>D</sup> type by a logistic regression model, whereas we classified sCJD subtype by CART, a supervised machine learning method. Third, we leveraged twice as many sCJD patients (487 vs 211), all examined with the DWI sequence, which is especially sensitive in detecting the signal abnormalities in the neocortex.<sup>23,38</sup> Our observations of the preferential participation of the neocortex over the striatum in MM(V)1, and of the rare striatal abnormalities in MM(V)2C, were both underestimated in the previous study likely because of the lack of the DWI sequence in many patients. Finally, our study takes advantage of the latest classification of sCJD subtypes that separate MV2C and MV2K.<sup>13</sup> Previously, these subtypes were comprised with no distinction in MV2 despite the marked dissimilarity.<sup>3,4</sup>

Our study showed that the distinctive features of these 2 subtypes can also be identified antemortem by diffusion MRI. A very recent study demonstrated that the occurrence of the 2 subtypes is directly related to the relative abundance of resPr<sup>D</sup>-129 M and resPr<sup>D</sup>-129 V allotypes, where resPr<sup>D</sup>-129 M dominated in MV2C and resPr<sup>D</sup>-129 V in MV2K.<sup>14</sup>

In the longitudinal component of this study, we have shown that signal abnormality on DWI extends to new brain regions in the first 3 months after symptom onset. In a prior cross-sectional MRI study, we demonstrated that the disease process is first detected in one distinct anatomical region or epicenter, and propagates along different trajectories that are subtype specific in subsequent stages.<sup>33</sup> The present study brings to the fore the impact that the appearance of new DWI hyperintensities associated with distinct stages of the disease may have on MRI diagnostic accuracy.

In agreement with Eisenmenger and colleagues,<sup>39</sup> the caudate was the region displaying the highest frequency of new abnormalities in subsequent diffusion MRI

examinations, followed by frontal cortex, putamen, and cingulate. Furthermore, our longitudinal results provided additional evidence that involvement of the striatum depends on the timing of the MRI and follows the parietal and frontal cortex in MM(V)1, whereas the striatum is more likely to precede propagation of disease to the frontal and parietal cortex in VV2 and MV2K. The latter finding is in agreement with Baiardi and colleagues.<sup>40</sup> Our diagnostic data-driven algorithms have been conceived on cross-sectional data of sCJD patients at different stages of the disease, enabling the exploitation of the time-dependent variations of the signal to further refine the diagnosis of subtype.

One inherent limitation of this study is the low case numbers of the rare subtypes in the training set, which decreased the discriminative ability of the decision trees for these variants, resulting in some overlap among subtypes. In PriSCA\_MRI, the rare VV1 subtype could not be distinguished from the most common MM(V)1 subtype, a limitation easily overcome by including the *PRNP129*. In PriSCA\_MRI + Gen, the low diagnostic performance for MV1 and MV2K is not surprising, because the MV genotype group (contrary to MM and VV) comprises 3 subtypes: MV1, MV2C, and MV2K. This condition would require a higher complexity of the decision tree, such as a higher number of internal nodes, to reach the same accuracy as in a binary classification. However, the relatively low sample size of the 3 MV variants in the training set limited the tree complexity and consequently resulted in low accuracy for the procedure.

A second possible limitation is the exclusion from this study of sCJD mixed phenotypes, which are characterized by the co-occurrence in variable ratios of resPrP<sup>D</sup> types 1 and 2 along with their matching histopathological phenotypes. The prevalence of type mixed forms following standard diagnostic procedures is significant: about 39% for all MM, 23% for all MV, and 23% for all VV sCJD cases.<sup>4,13,16,17</sup> However, it has been shown that both histopathological phenotypes are detectable at microscopic examination, hence likely by MRI, only in cases where the underrepresented resPrP<sup>D</sup> type accounts for more than 25% of the total resPrP.<sup>16,17</sup> Therefore, the mixed cases with <25% representation of one resPrP<sup>D</sup> type, which account for 60 to 70% of the total type mixed cases, likely will not interfere with the MRI diagnosis of subtype.<sup>16,17</sup> However, a study is needed to assess the MRI diagnostic capabilities of “true” type mixed cases, which may amount to about 8 to 12% of all sCJD cases.<sup>13,16,17</sup>

Another important issue is the experience and familiarity of the neuroradiologists with prion diseases and the correct interpretation of DWI signal hyperintensity. In our study, the MRI and histopathological examinations were interpreted by professionals with a high degree of

expertise in prion diseases. Authors of a recent study about retrospective reading of the original MRI reports showed that the DWI hyperintensities were rarely missed at the initial MRI, which was carried out in referring hospitals; however, the abnormalities were often not correctly interpreted at local hospitals by the radiologists, who often failed to raise the possibility of sCJD diagnosis.<sup>41</sup> The results of their and our study emphasize the importance of making radiologists and neurologists aware that sCJD presents with typical and early MRI findings that may suggest the diagnosis even before it is clinically suspected.<sup>42,43</sup>

We hope that our study will also stimulate developments that may further improve MRI diagnosis of prion and other neurodegenerative conditions. In prion disease, a major challenge is the in vivo measurement of microstructural alterations that prompt the diffusion MRI signal hyperintensity. Currently, spongiform degeneration with vacuole formation is considered to be the principal determinant of the DWI signal, whereas neuronal loss, astrogliosis, and kuru plaques would play a minor or no role.<sup>44–46</sup> In CJD, the size and micro configuration of the vacuoles allow for the easy histological distinction of some of the subtypes that could not be identified in the present study. For example, MM(V)2C features a spongiform degeneration characterized by large vacuoles often forming grapelike clusters, whereas MM(V)1 and VV1 vacuoles are small and of intermediate size, respectively. The addition of vacuolar size estimation with advanced diffusion MRI protocols would further and significantly improve the performance of PriSCA\_MRI.<sup>46,47</sup>

Finally, Mead et al have shown that *PRNP129* is an important determinant of the clinical decline rate when testing disease-modifying therapeutics in sCJD patients, and that the use of this genetic factor greatly improves statistical power in simulated trials.<sup>48</sup> We expect that the use of a more advanced procedure of subtype diagnosis, like PriSCA\_MRI + Gen, rather than codon 129 alone, will result in an even better stratification of sCJD patients for treatment trials.

In conclusion, this study demonstrates that diagnosis of the sCJD subtypes with diffusion MRI is achievable. Of the two procedures that we propose, the first, based on diffusion MRI examination alone, provides clinicians with a method of accurately diagnosing major sCJD subtypes at the bedside of individual patients; PriSCA\_MRI + Gen, which has higher and wider diagnostic capacities, is assisted by *PRNP129* data, which are easily available worldwide from prion surveillance centers. The accuracy of the two procedures did not change through MRI follow-up multiple examinations. Notably, the diffusion MRI examinations included in this study were acquired at many hospitals throughout the United States, using a

variety of MRI units, which bolsters the contention that our procedures may be transferable to academic as well as secondary care medical facilities.

## Acknowledgments

This study was conducted with support from the European Union's Horizon 2020 research and innovation program (grant agreement No. 666992, supporting A.B., R.P., J.B., F.M.D., and G.C.), the NIH (NINDS R01 NS083687, NIAID P01 AI106705, and NIAID P01 AI077774, supporting P.G.), the Charles S. Britton Fund (supporting P.G.), and the Centers for Disease Control and Prevention (NU38CK000480, supporting J.B., M.L.C., and B.S.A.). The findings and conclusions in this report are those of the authors and do not necessarily represent the official position of the Centers for Disease Control and Prevention, Atlanta, Georgia.

We thank the Creutzfeldt–Jakob Disease Foundation, and especially its President Debbie Yobs, for referring to the NPDPSC many of the patients recruited for this study.

## Author Contributions

A.B. and P.G. contributed to the conception and the design of the study. A.B., R.P., J.B., M.E.M.M., M.G., R.L., G.C., M.L.C., A.S., L.B.S., B.S.A., and P.G., contributed to the acquisition and analysis of the data. A.B., R.P., F.M.D., and P.G. contributed to drafting the text and preparing the figures.

## Potential Conflicts of Interest

Nothing to report.

## References

- Puoti G, Bizzi A, Forloni G, et al. Sporadic human prion diseases: molecular insights and diagnosis. *Lancet Neurol* 2012;11:618–628.
- Gambetti P, Cali I, Notari S, et al. Molecular biology and pathology of prion strains in sporadic human prion diseases. *Acta Neuropathol* 2011;121:79–90.
- Parchi P, De Boni L, Saverioni D, et al. Consensus classification of human prion disease histotypes allows reliable identification of molecular subtypes: an inter-rater study among surveillance centres in Europe and USA. *Acta Neuropathol* 2012;124:517–529.
- Zerr I, Parchi P. Sporadic Creutzfeldt-Jakob disease. In: Pocchiari M, Manson J, eds. *Handbook of clinical neurology*. Vol 153. Amsterdam, the Netherlands: Elsevier, 2018:155–174.
- Meyer A, Leigh D, Bagg CE. A rare presenile dementia associated with cortical blindness (Heidenhain's syndrome). *J Neurol Neurosurg Psychiatry* 1954;17:129–133.
- Brownell B, Oppenheimer DR. An ataxic form of subacute presenile poliоencephalopathy (Creutzfeldt-Jakob disease). *J Neurol Neurosurg Psychiatry* 1965;28:350–361.
- Cali I, Castellani R, Yuan J, et al. Classification of sporadic Creutzfeldt-Jakob disease revisited. *Brain* 2006;129:2266–2277.
- Badhwar A, McFall GP, Sapkota S, et al. A multiomics approach to heterogeneity in Alzheimer's disease: focused review and roadmap. *Brain* 2020;143:1315–1331.
- Parchi P, Castellani R, Capellari S, et al. Molecular basis of phenotypic variability in sporadic Creutzfeldt-Jakob disease. *Ann Neurol* 1996;39:767–778.
- Parchi P, Giese A, Capellari S, et al. Classification of sporadic Creutzfeldt-Jakob disease based on molecular and phenotypic analysis of 300 subjects. *Ann Neurol* 1999;46:224–233.
- Gambetti P, Kong Q, Zou W, et al. Sporadic and familial CJD: classification and characterisation. *Br Med Bull* 2003;66:213–239.
- Collins SJ, Sanchez-Juan P, Masters CL, et al. Determinants of diagnostic investigation sensitivities across the clinical spectrum of sporadic Creutzfeldt-Jakob disease. *Brain* 2006;129:2278–2287.
- Parchi P, Strammiello R, Notari S, et al. Incidence and spectrum of sporadic Creutzfeldt-Jakob disease variants with mixed phenotype and co-occurrence of PrPSc types: an updated classification. *Acta Neuropathol* 2009;118:659–671.
- Nemani SK, Xiao X, Cali I, et al. A novel mechanism of phenotypic heterogeneity in Creutzfeldt-Jakob disease. *Acta Neuropathol Commun* 2020;8:85.
- Parchi P, Strammiello R, Giese A, Kretschmar H. Phenotypic variability of sporadic human prion disease and its molecular basis: past, present, and future. *Acta Neuropathol* 2011;121:91–112.
- Cali I, Castellani R, Alshekhlee A, et al. Co-existence of scrapie prion protein types 1 and 2 in sporadic Creutzfeldt-Jakob disease: its effect on the phenotype and prion-type characteristics. *Brain* 2009;132:2643–2658.
- Cali I, Puoti G, Smucny J, et al. Co-existence of PrPD types 1 and 2 in sporadic Creutzfeldt-Jakob disease of the VV subgroup: phenotypic and prion protein characteristics. *Sci Rep* 2020;10:1503.
- Atarashi R, Satoh K, Sano K, et al. Ultrasensitive human prion detection in cerebrospinal fluid by real-time quaking-induced conversion. *Nat Med* 2011;17:175–178.
- Orrù CD, Bongiani M, Tonoli G, et al. A test for Creutzfeldt-Jakob disease using nasal brushings. *N Engl J Med* 2014;371:519–529.
- Orrù CD, Groveman BR, Hughson AG, et al. Rapid and sensitive RT-QuIC detection of human Creutzfeldt-Jakob disease using cerebrospinal fluid. *MBio* 2015;6:e02451–e02414.
- Vitali P, Maccagnano E, Caverzasi E, et al. Diffusion-weighted MRI hyperintensity patterns differentiate CJD from other rapid dementias. *Neurology* 2011;76:1711–1719.
- Piconi G, Peden AH, Barria MA, Green AJE. Epitope mapping of the protease resistant products of RT-QuIC does not allow the discrimination of sCJD subtypes. *PLoS One* 2019;14:e0218509.
- Meissner B, Kallenberg K, Sanchez-Juan P, et al. MRI lesion profiles in sporadic Creutzfeldt-Jakob disease. *Neurology* 2009;72:1994–2001.
- Foutz A, Appleby BS, Hamlin C, et al. Diagnostic and prognostic value of human prion detection in cerebrospinal fluid. *Ann Neurol* 2017;81:79–92.
- Bizzi A, Peoc'h K. Amended diagnostic protocol increases the early diagnosis of sporadic Creutzfeldt-Jakob disease. *Neurology* 2018;91:155–156.
- Zerr I, Kallenberg K, Summers DM, et al. Updated clinical diagnostic criteria for sporadic Creutzfeldt-Jakob disease. *Brain* 2009;132:2659–2668.
- Bizzi A, Pascuzzo R, Blevins J, et al. Evaluation of a new criterion for detecting prion disease with diffusion magnetic resonance imaging. *JAMA Neurol* 2020;77:1141–1149.

28. Gaudino S, Gangemi E, Colantonio R, et al. Neuroradiology of human prion diseases, diagnosis and differential diagnosis. *Radiol Med* 2017;122:369–385.
29. Manix M, Kalakoti P, Henry M, et al. Creutzfeldt-Jakob disease: updated diagnostic criteria, treatment algorithm, and the utility of brain biopsy. *Neurosurg Focus* 2015;39:E2.
30. Young GS, Geschwind MD, Fischbein NJ, et al. Diffusion-weighted and fluid-attenuated inversion recovery imaging in Creutzfeldt-Jakob disease: high sensitivity and specificity for diagnosis. *Am J Neuroradiol* 2005;26:1551–1562.
31. Meissner B, Kallenberg K, Sanchez-Juan P, et al. Isolated cortical signal increase on MR imaging as a frequent lesion pattern in sporadic Creutzfeldt-Jakob disease. *Am J Neuroradiol* 2008;29:1519–1524.
32. Lodi R, Parchi P, Tonon C, et al. Magnetic resonance diagnostic markers in clinically sporadic prion disease: a combined brain magnetic resonance imaging and spectroscopy study. *Brain* 2009;132:2669–2679.
33. Pascuzzo R, Oxtoby NP, Young AL, et al. Prion propagation estimated from brain diffusion MRI is subtype dependent in sporadic Creutzfeldt-Jakob disease. *Acta Neuropathol* 2020;140:169–181.
34. Breiman L, Friedman JH, Olshen RA, Stone CJ. *Classification and regression trees*. New York, NY: Taylor & Francis, 1984. <https://doi.org/10.1201/9781315139470>.
35. Kuhn M. Building predictive models in R using the caret package. *J Stat Softw* 2008;28:1–26.
36. Appleby BS, Connor A, Wang H. Therapeutic strategies for prion disease: a practical perspective. *Curr Opin Pharmacol* 2019;44:15–19.
37. Varges D, Manthey H, Heinemann U, et al. Doxycycline in early CJD: a double-blinded randomised phase II and observational study. *J Neurol Neurosurg Psychiatry* 2017;88:119–125.
38. Krasnianski A, Kallenberg K, Collie DA, et al. MRI in the classical MM1 and the atypical MV2 subtypes of sporadic CJD: an inter-observer agreement study. *Eur J Neurol* 2008;15:762–771.
39. Eisenmenger L, Porter M-C, Carswell CJ, et al. Evolution of diffusion-weighted magnetic resonance imaging signal abnormality in sporadic Creutzfeldt-Jakob disease, with histopathological correlation. *JAMA Neurol* 2016;73:76–84.
40. Baiardi S, Magherini A, Capellari S, et al. Towards an early clinical diagnosis of sporadic CJD VV2 (ataxic type). *J Neurol Neurosurg Psychiatry* 2017;88:764–772.
41. Carswell C, Thompson A, Lukic A, et al. MRI findings are often missed in the diagnosis of Creutzfeldt-Jakob disease. *BMC Neurol* 2012;12:153.
42. Satoh K, Nakaoka R, Nishiura Y, et al. Early detection of sporadic CJD by diffusion-weighted MRI before the onset of symptoms. *J Neurol Neurosurg Psychiatry* 2011;82:942–943.
43. Zanusso G, Camporese G, Ferrari S, et al. Long-term preclinical magnetic resonance imaging alterations in sporadic Creutzfeldt-Jakob disease. *Ann Neurol* 2016;80:629–632.
44. Mittal S, Farmer P, Kalina P, et al. Correlation of diffusion-weighted magnetic resonance imaging with neuropathology in Creutzfeldt-Jakob disease. *Arch Neurol* 2002;59:128–134.
45. Manners DN, Parchi P, Tonon C, et al. Pathologic correlates of diffusion MRI changes in Creutzfeldt-Jakob disease. *Neurology* 2009;72:1425–1431.
46. Figini M, Alexander DC, Redaelli V, et al. Mathematical models for the diffusion magnetic resonance signal abnormality in patients with prion diseases. *Neuroimage Clin* 2015;7:142–154.
47. Palombo M, Figini M, Pascuzzo R, et al. Improving strain diagnosis of prion disease by diffusion MRI and biophysical modelling. Abstract presented at: 27th ISMRM Annual Meeting and Exhibition; May 11–16, 2019; Montreal, QC, Canada; abstract 0963. <https://discovery.ucl.ac.uk/id/eprint/10074392/>
48. Mead S, Burnell M, Lowe J, et al. Clinical trial simulations based on genetic stratification and the natural history of a functional outcome measure in Creutzfeldt-Jakob disease. *JAMA Neurol* 2016;73:447–455.